applied optics

Ion beam figuring approach for thermally sensitive space optics

Xiaolin Yin,[1,3] Weijie Deng,[2,3,*] Wa Tang,[2,3] Binzhi Zhang,[2,3] Donglin Xue,[2,3] Feng Zhang,[2,3] and Xuejun Zhang[2,3]

[1]University of Chinese Academy of Sciences, Beijing 100039, China
[2]Changchun Institute of Optics, Fine Mechanics and Physics, Chinese Academy of Sciences, Changchun 130033, China
[3]Key Laboratory of Optical System Advanced Manufacturing Technology, Chinese Academy of Sciences, Changchun 130033, China
*Corresponding author: mr-deng@163.com

Received 28 July 2016; revised 2 September 2016; accepted 5 September 2016; posted 7 September 2016 (Doc. ID 272676); published 29 September 2016

During the ion beam figuring (IBF) of a space mirror, thermal radiation of the neutral filament and particle collisions will heat the mirror. The adhesive layer used to bond the metal parts and the mirror is very sensitive to temperature rise. When the temperature exceeds the designed value, the mirror surface shape will change markedly because of the thermal deformation and stress release of the adhesive layer, thereby reducing the IBF accuracy. To suppress the thermal effect, we analyzed the heat generation mechanism. By using thermal radiation theory, we established a thermal radiation model of the neutral filament. Additionally, we acquired a surface-type Gaussian heat source model of the ion beam sputtering based on the removal function and Faraday scan result. Using the finite-element-method software ABAQUS, we developed a method that can simulate the thermal effect of the IBF for the full path and all dwell times. Based on the thermal model, which was experimentally confirmed, we simulated the thermal effects for a 675 mm × 374 mm rectangular SiC space mirror. By optimizing the dwell time distribution, the peak temperature value of the adhesive layer during the figuring process was reduced under the designed value. After one round of figuring, the RMS value of the surface error changed from 0.094 to 0.015λ (λ = 632.8 nm), which proved the effectiveness of the thermal analysis and suppression method.

OCIS codes: (220.0220) Optical design and fabrication; (220.5450) Polishing; (230.4040) Mirrors; (140.6810) Thermal effects.

http://dx.doi.org/10.1364/AO.55.008049

1. INTRODUCTION

With the fast development of modern space optics systems, space mirror surface accuracy is required to achieve nanometer-scale precision or even sub-nanometer-scale precision [1–3]. Since the 1970s, ion beam figuring (IBF) technology has been successfully applied in the polishing process of space mirrors, which can theoretically achieve atomic-scale removal [4,5]. The ion beam source (IBS) is controlled by its motion system to realize different processing paths and dwell time distributions over the mirror. In the meantime, the inert gas ions (mostly Argon ions) with certain energy and spatial distribution interact with the surface atoms, which is called sputtering, to realize the desired material removal [6–8].

However, IBF technology also has some disadvantages, the main one being that the mirror surface temperature greatly increases with ion beam bombardment and thermal radiation of the filament, which leads to different degrees of deformation or damage to the mirror, especially the flexible support. Currently, when engineers design space mirror supports, they prefer to use bonding approaches to connect the metal parts with the mirror [9,10]. When the temperature is very high, the mirror surface shape changes markedly because of the thermal deformation and stress release of the adhesive layer [11,12], thereby reducing the IBF accuracy.

To suppress the thermal effect of IBF, we must first know the temperature distribution of the mirror in the IBF process. Second, we must develop a new figuring method to decrease the high temperature. Patrick Gailly, from Centre Spatial de Liège, used an infrared thermal imaging camera to monitor the surface temperature of a BK7 and fused silica mirror and analyzed the effect of high temperature and the temperature gradient [13]. Xie from the National University of Defense Technology employed a filtered IBF machining flow to make the surface temperature more uniform, which can decrease the thermal stress by 20% [14,15]. These relevant studies mainly focused on high-thermal-expansion optical components like BK7 and have been successfully applied in the IBF process. However, in a space mirror's actual IBF, the temperature of

the adhesive layer area cannot be monitored by infrared thermal imaging cameras. The temperature of the adhesive layer also must be strictly adjusted under the designed value because of its unpredictable effect on the surface shape, as mentioned earlier. Therefore, the thermal suppression method must be further discussed.

In this study, we developed a full-path simulation method based on a moving heat source to predict the temperature distribution of a space mirror during IBF. In addition, we have proposed the multistep figuring method for thermal suppression of the adhesive layer temperature. Finally, we conducted an experiment on a 675 mm × 374 mm rectangular SiC space mirror to prove the effectiveness of the thermal analysis and suppression method.

In Section 2, we have analyzed the heat-generation mechanism of a space mirror during IBF and established the heat source model of IBF. In Section 3, we have proposed the full-path simulation method. In Section 4, we have described a verification experiment for the heat source. In Section 5, we applied the full-path simulation and the multistep figuring method to a 675 mm × 374 mm rectangular SiC space mirror and presented the results. Section 6 gives our conclusions.

2. ESTABLISHMENT OF HEAT SOURCE MODEL

Because IBF is performed in a vacuum, the heat absorbed by the mirror mainly consists of the energy deposited by the ion beam and the thermal radiation of the neutral filament and the inner surface of the vacuum chamber. Owing to the large heat capacity, the thermal radiation of the vacuum chamber on the mirror can be neglected.

A. Thermal Radiation of the Filament

Under vacuum conditions, the filament can only heat the surface of the mirror through thermal radiation and the energy can be calculated with the formula (1)

$$Q = \epsilon\delta SF(T_1^4 - T_2^4), \tag{1}$$

where ϵ is the emissivity of the filament, δ is the Stefan–Boltzmann constant, $\delta = 5.67 \times 10^{-8}\ \mathrm{W/m^2 \cdot K^4}$, S is the surface area of the filament, F is the radiation angle factor, and T_1 and T_2 are the temperature of the filament surface and the mirror surface, respectively.

However, in practical situations, the filament is separated from the mirror by the diaphragm, as shown in Fig. 1. Therefore, the heat can only be transferred to the mirror surface through the hole in the diaphragm, which substantially decreases the radiant energy of the filament. The temperature of the filament is usually approximately 2500 K, and the length and the diameter of the filament are 125.6 mm and 0.2 mm, respectively. Using simulation and calculation, Fig. 2 shows that we obtained the steady temperature distribution contributed by the filament during IBF. From the simulation results, it is evident that the thermal effect of the filament is limited by the shelter of the diaphragm, but which cannot be overcome considering the modeling accuracy. Therefore, we assumed the thermal effect of the filament to be a uniform surface heat source q_f and we could obtain this value from the simulation.

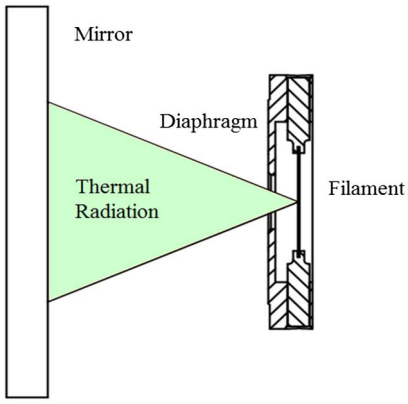

Fig. 1. Relative position of the filament and the space mirror.

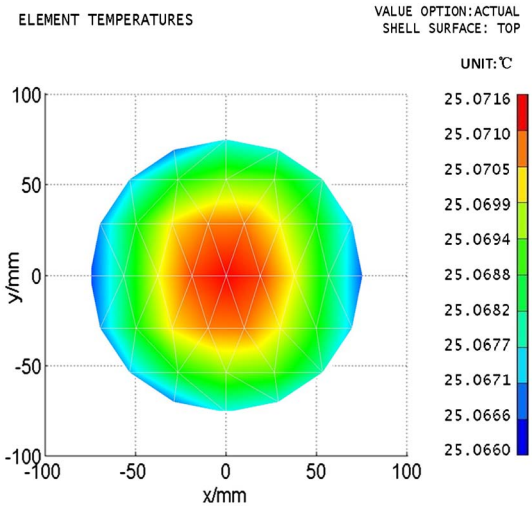

Fig. 2. Temperature distribution contributed by the filament (in °C).

B. Energy Deposition of the Ion Beam

Currently, Si-modified silicon carbide (SiC) is widely used in the manufacturing of space mirrors because of its excellent physical and optical performance [16]. Si atoms are removed by sputtering, which occurs when an ion beam bombards the Si-modified mirror surface. As a result, the energy of the ion beam is deposited on the mirror surface [17]. One part is used to provide sufficient energy for the surface atoms of the mirror to break the surface bonds so as to realize atomic removal, while the other part is consumed in the mirror surface through ionization, phonons, or other forms. Ignoring the effect of radiation and secondary electron emission, all the energy loss is ultimately converted into heat.

Since the ion beam density has a Gaussian distribution and the power density is directly proportional to the ion beam density, the power density also exhibits a Gaussian distribution. The ion beam sputtering software SRIM (the stopping and range of ions in matter) can obtain the absorbed energy e_2 for incident ions with energy e_1 [18]. Figure 3 displays the result. In this paper, e_1 is 1000 eV and e_2 is the integral of the

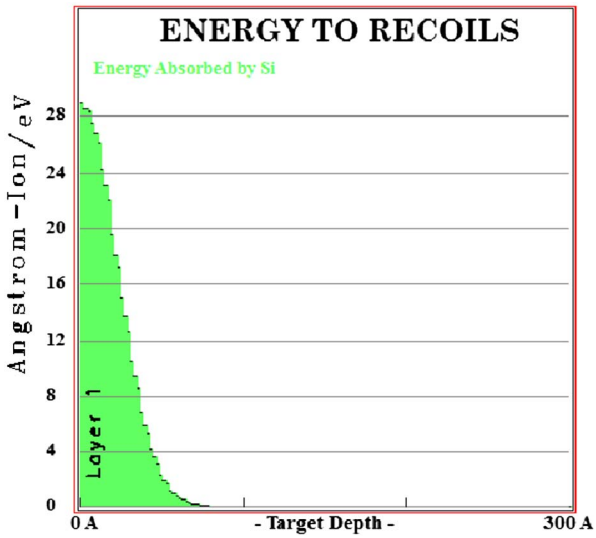

Fig. 3. Energy absorbed by Si.

curve in Fig. 3, which is 843 eV. Furthermore, the energy is proportional to the power, which means that the distribution of the heat source (absorbed energy) is also a Gaussian one. In addition, the physical sputtering occurs in a region with a very small depth-to-width ratio. Therefore, the heat flux produced by the ion beam current can be fitted according to the surface-type and Gaussian heat source model

$$q(r) = q_{\max} e^{-r^2/(2\sigma^2)}, \tag{2}$$

where r is the radial distance from a point to the center of the heat source, $q(r)$ is the surface heat flux at radius r, $q_{\max}$ is the maximum heat flux at the heat source center, and σ is the standard deviation of the Gaussian distribution, which can be obtained from the removal function of IBF for space mirrors.

It is possible to determine the maximum heat flux at the heat source center according to the results of the Faraday scan and the SRIM simulation.

The Faraday cup is a cup-shaped metal vacuum detector employed for density measurements of incident charged particles. We can use the measured current to determine the number of incident electrons or ions. Therefore, we can obtain the maximum beam current density $I_{\max}$ from the Faraday scan results, with which the corresponding power density can be achieved by

$$P = U_B I_{\max} \tag{3}$$

and the maximum heat flux at heat source center is

$$q_{\max} = (e_2/e_1)P = (e_2/e_1)U_B I_{\max}. \tag{4}$$

3. FULL-PATH SIMULATION BASED ON MOVING HEAT SOURCE

In the process of IBF, the IBS moves along the planned path (a meander path was adopted in this study, as shown in Fig. 4) to dwell over the mirror surface. We can obtain the dwell time distribution from the initial surface error of the mirror and the removal function by deconvolution [19]

$$S_d(x,y) = R(x,y) ** T_c(x,y), \tag{5}$$

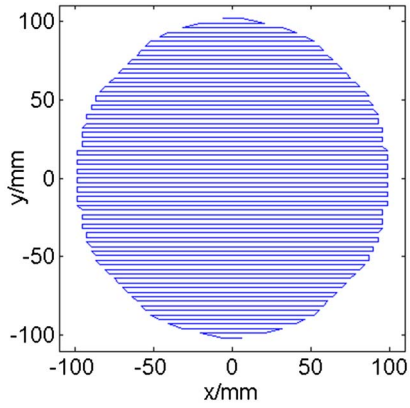

Fig. 4. Meander path of a 150 mm flat mirror.

where $S_d(x,y)$ is the desired surface error distribution to remove, $R(x,y)$ is the removal function, ** denotes the two-dimensional convolution, and $T_c(x,y)$ is the calculated dwell time distribution, which is not uniform because the initial surface error is irregular.

Therefore, to simulate the thermal effect of IBF, we must conduct a full-path simulation based on a moving heat source, which means the heat source must also move along the meander path and obey the dwell distribution of $T_c(x,y)$. By calling a subroutine compiled in FORTRAN, the finite-element method (FEM) software ABAQUS can determine the motion and the dwell time of the heat source.

To accurately simulate the change of temperature during IBF, we also need a realistic heat transfer model. For three-dimensional Cartesian coordinates, the equations describing the transient heat conduction in domain V are

$$\rho c \frac{\partial u}{\partial t} - k\left(\frac{\partial^2 u}{\partial x^2} + \frac{\partial^2 u}{\partial y^2} + \frac{\partial^2 u}{\partial z^2}\right) = 0, \tag{6}$$

where u is the temperature, k is the thermal conductivity, ρ is the density, and c is the specific heat.

If all the boundary conditions of the mirror in domain V are assumed to be Γ, the initial temperature of the boundary Γ_u (except the area being figured) is known as

$$u = u_0. \tag{7}$$

The boundary condition of the area being figured, Γ_q, is also known as

$$n_x k_x \frac{\partial u}{\partial x} + n_y k_y \frac{\partial u}{\partial y} + n_z k_z \frac{\partial u}{\partial z} = q(r), \tag{8}$$

where $q(r)$ is the flux of the boundary Γ_q, and n_x, n_y, and n_z are the direction cosines of the boundary surface normal in the x, y, and z directions, respectively.

These two parts constitute the complete boundary of the mirror

$$\Gamma = \Gamma_u + \Gamma_q. \tag{9}$$

4. EXPERIMENTAL VERIFICATION OF HEAT SOURCE MODEL

To verify the accuracy of the heat source model, we conducted a full-path simulation and a temperature measurement on a piece of a 150 mm Si-modified SiC mirror.

First, we tested the removal function with a RF IBS in the IBF-1500 (NTG Neue Technologien GmbH, Gelnhausen, Germany). The ion energy and the ion current of the ion beam used are 1000 eV and 28 mA, respectively. During the test, the distance between the IBS and the mirror surface was 80 mm and the vacuum degree of the chamber was 3.9×10^{-5} mbar. The model of the removal function was fitted with a Gaussian distribution, as shown in Fig. 5(a); the standard deviation is $\sigma_x = 10.823$ mm and $\sigma_y = 10.688$ mm and the RMS value of the fitting residual is 5.46 nm.

The Faraday scan result shows that the maximum beam current density $I_{\max}$ was 4.65 mA/cm^2. According to Eqs. (1–5), we can obtain the heat source model, and the calculation result is given in Eq. (10) and Fig. 5(b):

$$q(r) = q_{\max} e^{-(x-x_0)^2/(2\sigma_x^2)} e^{-(y-y_0)^2/(2\sigma_y^2)} + q_f. \quad (10)$$

We simplified two aspects of the model used in the simulation and experiment to improve the accuracy of the verification experiment. First, as shown in Fig. 6, a mirror without support was used, which simplified the FEM model. By using a muscovite thermal baffle, the heat of the mirror was insulated from other heat sink parts so that the heat dissipation in the mirror occurred only through thermal radiation; consequently, the heat transfer model was simplified. Second, to simplify the boundary conditions, we used a uniform dwell time distribution, as shown in Fig. 7. The dwell time at each figuring point was 348 ms and the total figuring time was 31 min. When the IBS arrived to the edge, it moved rapidly to reduce the effect of the thermal radiation on the mirror.

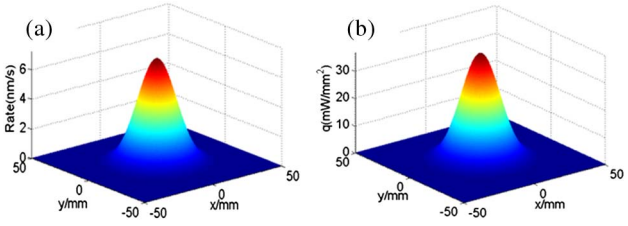

Fig. 5. (a) Fitting result of removal function (in nm/s), (b) calculation result of the heat source model (in mW/mm^2).

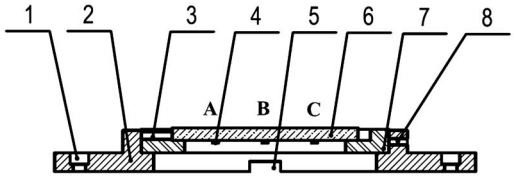

Fig. 6. Configuration of experimental equipment: 1: counter bores, 2: aluminum alloy base, 3: fixing holes, 4: sheet-type platinum resistance temperature sensors, 5: wiring troughs, 6: mirror, 7: muscovite thermal baffle, and 8: muscovite fixing holes.

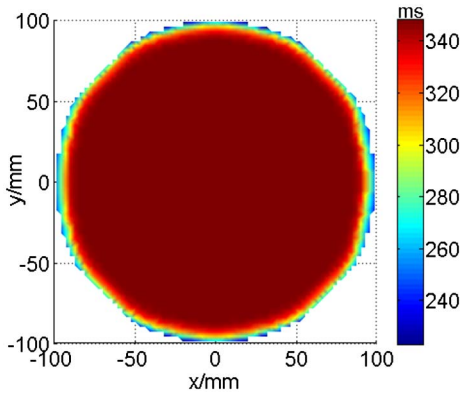

Fig. 7. Dwell time distribution of the IBS over the mirror.

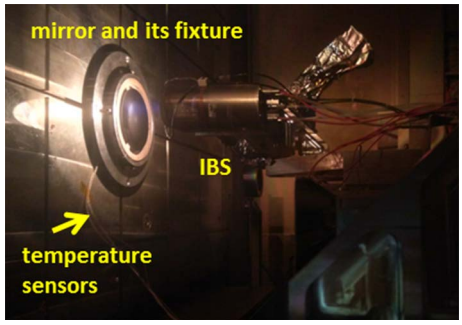

Fig. 8. Temperature measurement experiment on SiC mirror.

As shown in Fig. 8, we performed the IBF experiment on a 150 mm SiC mirror according to the IBS parameters and the dwell time distribution mentioned earlier. Sheet-type platinum resistance temperature sensors recorded the temperature changes at points A, B, and C along the horizontal diameter direction (Fig. 6), where point B is the center of the mirror and $AB = BC = 40$ mm. Additionally, we conducted the full-path simulation using ABAQUS. Our results show that the peak values at point A, B and C are similar, owing to the good thermal conductivity of SiC material. The temperature changes of points A, B, and C are displayed in Figs. 9, 10, and 11, respectively. The red and black curves belong to the left axis while the blue curve belongs to the right axis. The

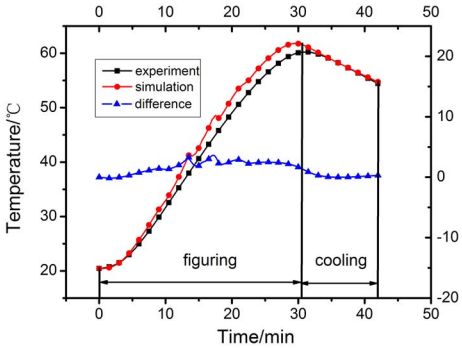

Fig. 9. Temperature measurement and simulation at point A.

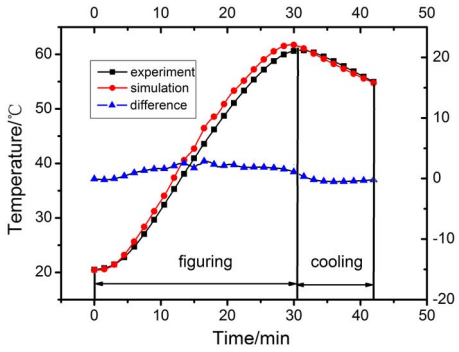

Fig. 10. Temperature measurement and simulation at point B.

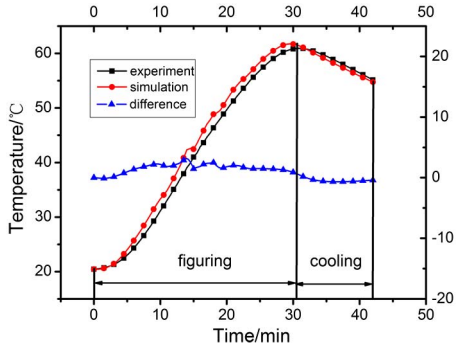

Fig. 11. Temperature measurement and simulation at point C.

difference between the simulation and the experiment is indicated by the blue curve and the mean value of the differences was 1.09°C, 0.93°C, and 0.69°C, respectively, which are reasonable when considering factors like the accuracy, delay, and contact thermal resistance of the sensors.

5. IBF OF SPACE MIRROR WITH THERMAL SUPPRESSION

We conducted the IBF of a 675 mm × 374 mm rectangular SiC space mirror with the proposed removal function model and heat source model. Figure 12 shows the initial surface error before IBF. Figure 13 provides the dwell time distribution of complete convergence. Using the full-path simulation, we obtained the temperature distribution, as shown in Fig. 14.

The simulation results demonstrate that the mirror temperature reached the peak value 71.2°C at the step time 24240 s. Figure 15 provides the temperature change of one of the adhesive layers. The peak value of the layer temperature is 52°C. Considering the stress release, the designed temperature value is under 40°C. Therefore, the temperature of the adhesive layer during IBF must be reduced. From the theoretical analysis and experimental results, we can conclude that the heat source is inevitable because it is accompanied by the material removal. Furthermore, the addition of a cooling system is complex and expensive because of the vacuum environment and the different sizes and structures of the space mirrors. Therefore, this study mainly achieved the goal of

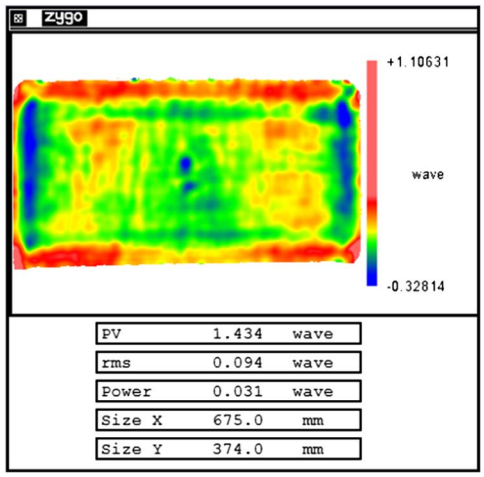

Fig. 12. Initial surface error of the mirror.

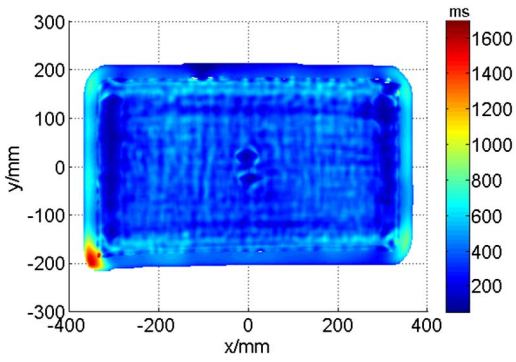

Fig. 13. Dwell time distribution of complete convergence (in ms).

thermal suppression through the control of a single figuring time $T(x, y)$.

We introduced the time control factor n in the calculation process to enlarge the removal function $R(x, y)$. Based on the new removal function $R_n(x, y)$, we can acquire the optimized

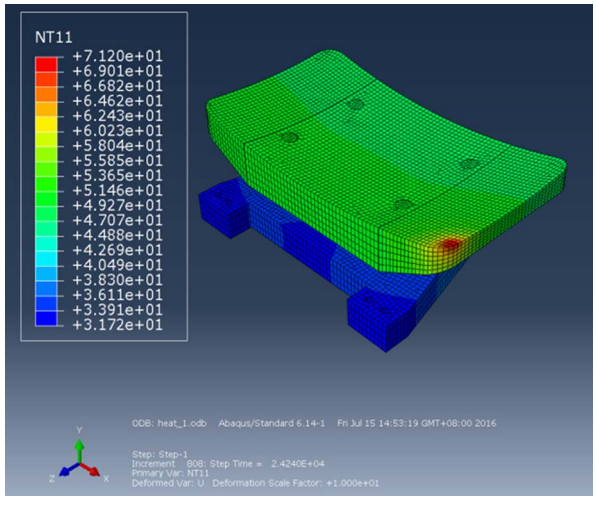

Fig. 14. Temperature distribution of complete convergence (in °C).

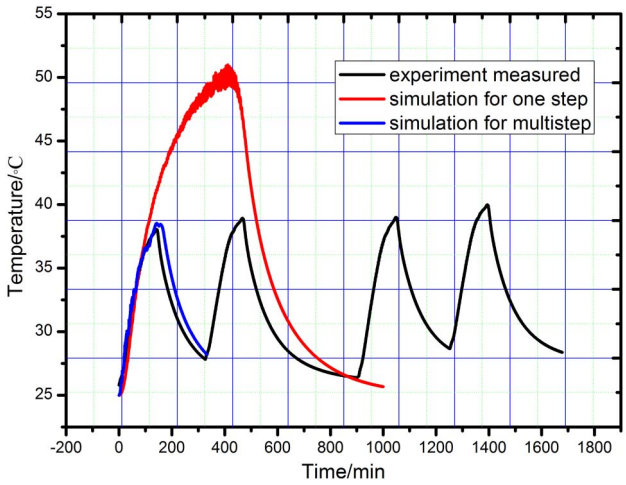

Fig. 15. Temperature change of the adhesive layer.

dwell time distribution $T_n(x, y)$ to conduct the full-path simulation. If the simulation results meet the requirements of the designed temperature, the space mirror can undergo IBF for n times. For the second and later times, the figuring process cannot be started until the mirror is passively cooled down to room temperature. If the simulation results do not satisfy the requirements, the time control factor n must be increased to perform the iterative computation again. Figure 16 presents the flow diagram of the IBF with thermal suppression.

After the iterative calculation, we determined that the time control factor n of the mirror is 4. Figure 17 shows the dwell time distribution of a single figuring. By simulating with the optimized dwell time distribution, we reduced the highest temperature of the adhesive layer to 37°C, which is shown

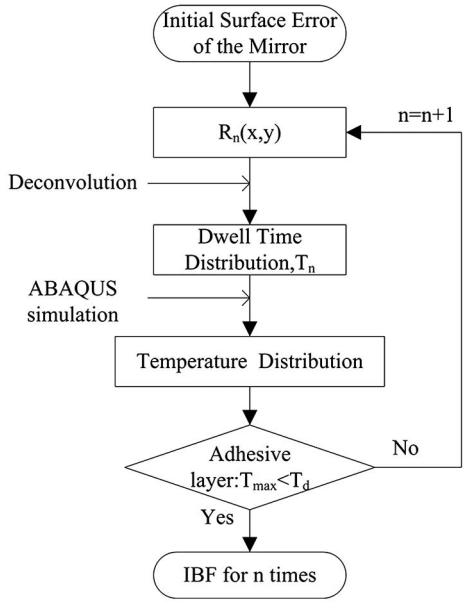

Fig. 16. IBF flow for the space mirror by introducing time control factor and full path simulation.

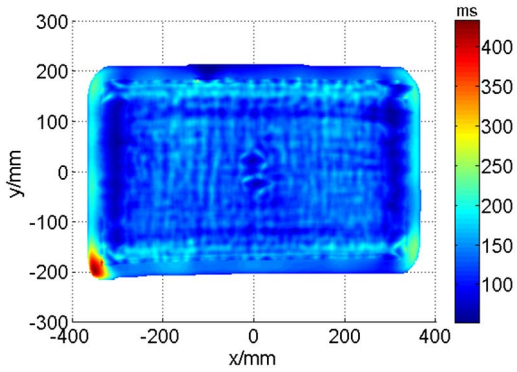

Fig. 17. Dwell time distribution of multistep convergence (in ms).

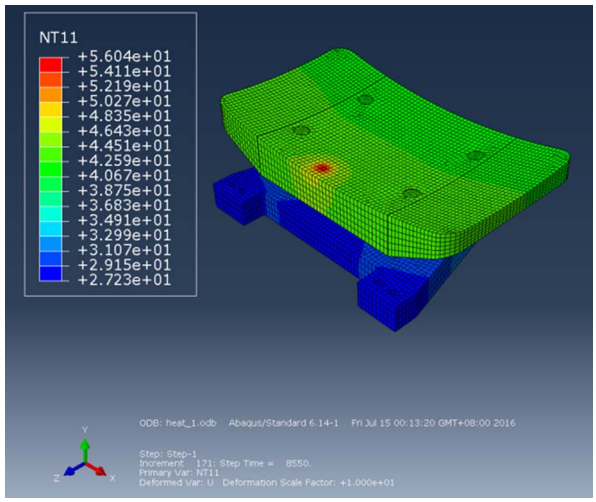

Fig. 18. Temperature distribution of multistep convergence (in °C).

in Figs. 15 and 18. As Figs. 19 and 20 show, after a round comprising four steps of figuring, the RMS value of the surface error converges from 0.094 to 0.015λ (λ = 632.8 nm). This result proves, to a certain degree, the effectiveness of the thermal analysis and suppression method.

Fig. 19. Figuring experiment in the IBF-1500.

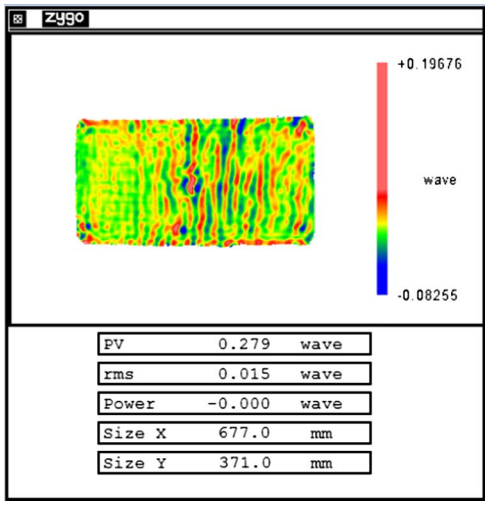

Fig. 20. Surface error after a round of four steps of figuring.

6. CONCLUSION

In IBF, the heat source mainly comprises the thermal radiation of the neutral filament and the energy deposition of the ion beam. Regarding the space mirror, in this study we investigated the temperature control of the adhesive layer. To achieve thermal suppression during IBF, we first modeled the heat source of the ion beam deposition with a novel method based on the removal function and Faraday cup scanning. Second, we proposed a full-path simulation using ABAQUS to predict the temperature distribution of IBF for the entire path and all dwell times. With a specially designed experiment and simulation, we confirmed the heat source model to be realistic. Finally, we applied a multistep figuring method on a 675 mm × 371 mm rectangular SiC space mirror by introducing the time control factor. By optimizing the dwell time distribution, the temperature of the mirror, especially the adhesive layer, can be fairly controlled under the designed level. We reduced the peak temperature value of the adhesive layer from 52°C to 37°C in a single figuring process. The figuring results indicate that the thermal analysis and suppression method is correct and effective to ensure the figuring accuracy of the space mirror.

Funding. National Natural Science Foundation of China (NSFC) (61210015, 61605202).

REFERENCES

1. A. M. Hoogstrate, C. V. Drunen, B. V. Venrooy, and R. Henselmans, "Manufacturing of high-precision aspherical and freeform optics," Proc. SPIE **8450**, 84502Q (2012).
2. F. Allenstein and S. Kiontke, "Ion beam figuring (IBF) for high precision optics," Proc. SPIE **7591**, 75910Y (2010).
3. W. Liao, Y. Dai, X. Nie, X. Xie, and C. Song, "Rapid fabrication technique for nanometer-precision aspherical surfaces," Appl. Opt. **54**, 1629–1638 (2015).
4. L. N. Allen and H. W. Romig, "Demonstration of an ion-figuring process," Proc. SPIE **1333**, 164–170 (1990).
5. L. N. Allen, J. J. Hannon, and R. W. Wambach, "Final surface error correction of an off-axis aspheric petal by ion figuring," Proc. SPIE **1543**, 190–200 (1991).
6. T. Haensel, A. Nickel, and A. Schindler, "Ion beam figuring of strongly curved surfaces with a (x, y, z) linear three axes system," in *Frontiers in Optics 2008/Laser Science XXIV/Plasmonics and Metamaterials/Optical Fabrication and Testing* OSA Technical Digest (CD) (Optical Society of America, 2008), paper JWD6.
7. S. Malobabic, M. Jupé, and D. Ristau, "Spatial separation effects in a guiding procedure in a modified ion-beam-sputtering process," Light Sci. Appl. **5**, 3 (2015).
8. W. Guo, Y. Zheng, H. Wang, and B. Liang, "Pilot study for ion beam figuring process," Proc. SPIE **7655**, 765506 (2010).
9. O. Vlasenko, A. Zverev, and M. Sachkov, "Using the DP-190 glue for adhesive attachment of a large space mirror and its rim," Proc. SPIE **915131**, 91513I (2014).
10. Y. Guan, "Optimum design of adhesive bonds in the space mirror," J. Mac. Des. **28**, 72 (2011).
11. D. Dong, Z. Li, R. Li, Y. Fan, and X. Zhang, "Effect of adhesive curing on the mirror surface shape simulation and test," Opt. Precis. Eng. **22**, 2698–2707 (2014).
12. S. Jia, W. Huang, and W. Pang, "Influence of adhesive thickness on surface deformation of mirror supported by three-point mount," Opt. Precis. Eng. **23**, 2005–2012 (2015).
13. P. Gailly, J.-P. Collette, L. F. Renson, and J. P. Tock, "Ion beam figuring of small BK7 and Zerodur optics: thermal effects," Proc. SPIE **3739**, 124–131 (1999).
14. X. Xie, H. Yu, L. Zhou, Y. Dai, and S. Li, "High thermal expansion optical component machined by ion beam figuring," Opt. Eng. **51**, 013401 (2012).
15. Z. Yuan, Y. Dai, and X. Xie, "Numerical simulation on the thermal deposition of optical surface irradiated by low energy ion beam in ion beam figuring," Acta Phys. Sinica **61**, 22–24 (2012).
16. M. A. Ealey, "Design, fabrication, and test of a meter-class reaction bonded SiC mirror blank," Proc. SPIE **2543**, 254312 (1995).
17. M. T. Myers, B. H. Sencer, and L. Shao, "Multi-scale modeling of localized heating caused by ion bombardment," Nucl. Instrum. Methods Phys. Res. Sect. B **272**, 165–168 (2012).
18. J. F. Ziegler, M. D. Ziegler, and J. P. Biersack, "SRIM–The stopping and range of ions in matter (2010)," Nucl. Instrum. Methods Phys. Res. Sect. B **268**, 1818–1823 (2010).
19. J. Wu, Z. Lu, and H. Zhang, "Dwell time algorithm in ion beam figuring," Appl. Opt. **48**, 3930–3937 (2009).